Published in final edited form as:
Ultrason Imaging. 2009 July ; 31(3): 183–200.

Novel Acoustic Radiation Force Impulse Imaging Methods for Visualization of Rapidly Moving Tissue

Stephen J. Hsu[1], **Richard R. Bouchard**[1], **Douglas M. Dumont**[1], **Cheng W. Ong**[1], **Patrick D. Wolf**[1], and **Gregg E. Trahey**[1,2]

Stephen J. Hsu: stephen.j.hsu@duke.edu; Richard R. Bouchard: ; Douglas M. Dumont: ; Cheng W. Ong: ; Patrick D. Wolf: ; Gregg E. Trahey:

[1] Department of Biomedical Engineering, Duke University, Durham, NC, 27708

[2] Department of Radiology, Duke University, Durham, NC, 27708

Abstract

Acoustic radiation force impulse (ARFI) imaging has been demonstrated to be capable of visualizing changes in local myocardial stiffness through a normal cardiac cycle. As a beating heart involves rapidly-moving tissue with cyclically-varying myocardial stiffness, it is desirable to form images with high frame rates and minimize susceptibility to motion artifacts.

Three novel ARFI imaging methods, pre-excitation displacement estimation, parallel-transmit excitation and parallel-transmit tracking, were implemented. Along with parallel-receive, ECG-gating and multiplexed imaging, these new techniques were used to form high-quality, high-resolution epicardial ARFI images. Three-line M-mode, extended ECG-gated three-line M-mode and ECG-gated two-dimensional ARFI imaging sequences were developed to address specific challenges related to cardiac imaging. *In vivo* epicardial ARFI images of an *ovine* heart were formed using these sequences and the quality and utility of the resultant ARFI-induced displacement curves were evaluated. The ARFI-induced displacement curves demonstrate the potential for ARFI imaging to provide new and unique information into myocardial stiffness with high temporal and spatial resolution.

Keywords

Acoustic radiation force impulse imaging; echocardiography; motion filter; ultrasound

I. INTRODUCTION

Acoustic radiation force impulse (ARFI) imaging transmits high-intensity acoustic pulses to create and track small displacements within soft tissue. Within a homogeneous, isotropic, viscous and dissipative medium, the radiation force (F) generated by these high-intensity acoustic pulses at any point within the material is described as:[1–3]

$$F(\vec{r},t)=\frac{2\alpha I(\vec{r},t)}{c} \quad (1)$$

Correspondence to: Stephen J. Hsu, stephen.j.hsu@duke.edu.

where α and *c* are the attenuation coefficient and speed of sound of the material and $I(\vec{r},t)$ is the local time-averaged acoustic intensity of the acoustic pulse at that point. The tissue response and recovery from this radiation force pulse is partially determined by the elastic properties of the material – most notably that stiffer tissue displaces less than more compliant tissue. ARFI imaging tracks these tissue responses to radiation force excitations to gain insight into the local elastic properties of the material.[4, 5]

As ARFI-induced displacements are typically small (~10 μm), a fundamental concern in ARFI imaging is the reduction of displacement artifacts not caused by the ARFI excitation. The primary sources of these external displacements are associated with transducer motion and physiological motion. Transducer motion can be minimized by stabilizing the probe with either a steady hand or an apparatus that holds the probe stationary. However, ARFI imaging in the presence of moderate to great physiological motion requires more sophisticated measures.

The main sources of physiological motion are respiratory and cardiovascular. Accordingly, the applications of ARFI imaging most affected by physiological motion are abdominal and cardiovascular imaging. Within a breath, the thoracic diaphragm can displace up to 4 cm, causing the entire abdomen to displace with it.[6] This is particularly a concern in hepatic ARFI imaging where abdominal motion is principally normal to the correlation (axial) dimension. This motion contributes to pulse-to-pulse decorrelation and motion artifacts that are difficult to remove.[7, 8] In cardiovascular ARFI imaging, physiological motion is caused by myocardial contraction and the pulsatile flow of blood, with myocardial tissue velocities exceeding 3 cm/s during ejection and filling.[9–11] Vascular distention due to blood flow and changes in blood pressure are typically small, with the maximum distention of larger vessels approximately 1 mm, and vary from vessel to vessel.[12]

Cardiac ARFI imaging faces unique challenges associated with the contraction of the heart during data acquisition. Traditional ultrasonic imaging of the heart has found widespread use in the evaluation of the myocardial health. The implementation of speckle tracking and Doppler imaging techniques on these echocardiograms has also resulted in motion-based analysis of the heart. As a result, extensive research in tissue motion imaging and myocardial elastography has provided additional insight into myocardial function and performance.[9, 13, 14] However, these methods rely on the natural motion of the heart for their measurements, and therefore, may be influenced by myriad factors external to the fundamental mechanical properties and functionality of the myocardium, including blood pressure, load, and heart rate. The radiation-force excitations used in ARFI imaging are independent of these additional physiological variables.

For single image acquisitions, breath holds and ECG-gating can be used to help minimize motion artifacts. Interpolation-based motion filters have been developed and proven to be effective in removing motion artifacts in virtually every application of ARFI imaging.[15–18] However, when continuously sampling ARFI images within a rapidly-moving environment, imaging sequence advancements and modifications that maintain image quality while increasing the sampling capability are necessary. The thermal exposure to the subject and the transducer due to repeated transmissions of the radiation force pulse must also be considered.[19, 20]

Acquisition times for traditional two-dimensional (2-D) ARFI images are approximately 200 ms, corresponding to a maximum frame rate of 5 Hz. These long acquisition times allow for greater variability in tissue velocities and evolving tissue stiffnesses within the acquisition and increase the likelihood of spatial artifacts within the images. As a result, initial investigations into cardiac ARFI imaging utilized parallel-receive and multiplexed imaging to shorten acquisition times and reduce thermal exposure to both the transducer and tissue and yielded 2-

D ARFI images of a beating heart sampled at 10 Hz.[21–23] To further increase sampling rates, spatial sampling was sacrificed and ARFI excitations were transmitted at three spatial locations only. These three-line M-mode ARFI images were sampled at 40 Hz.

In order to further increase the applicability of ARFI imaging, additional improvements to the imaging sequences are needed to provide finer sampling with better spatial and temporal resolution and interbeam consistency so that more detailed information can be gleaned from the ARFI images and displacement data. We present three new ARFI imaging methods designed to image rapidly-moving and changing myocardium. They are parallel-transmit excitation, parallel-transmit tracking and pre-excitation tracking. The significance and relevance of these new methods of cardiac ARFI imaging are demonstrated.

II. METHODS

Imaging methods

A detailed description of traditional ARFI imaging sequences is provided by Nightingale et al. [5] The sequences presented and used in this paper are derivatives of these fundamental ARFI imaging sequences; however, they include several variants and modifications that allow them to be better suited for cardiac ARFI imaging. Imaging acquisitions were performed with the Siemens SONOLINE Antares™ ultrasound system (Siemens Healthcare, Ultrasound Business Unit, Mountain View, CA) and a VF10-5, linear ultrasound transducer. Images were formed at a center frequency of 6.67 MHz and acquired using the Siemens Ultrasonic Research Interface™ to record in-phase (I) and quadrature (Q) data from the received echoes.

Due to a high number of false peaks when performing correlation-based displacement estimation within the large search regions necessary for imaging environments of increased motion, displacements were estimated from the I/Q data using a phase-shift estimation algorithm and a 0.33 mm axial kernel.[24] To correct for phase wrapping and aliasing errors from this algorithm, displacement discontinuities greater than half of a wavelength were shifted a full wavelength in the opposite direction. Motion filters were used to separate ARFI-induced displacements from the natural cardiac motion of a heartbeat. Two-dimensional ARFI images and ARFI-induced displacement curves were generated by taking displacements measured at specific times after cessation of the radiation force pulse for each lateral location. Two-dimensional ARFI images were also median filtered using a 0.9 mm × 0.9 mm kernel. ARFI-induced displacement plots were temporally low-pass filtered with a 5.8 ms mean filter.

In this paper, several novel ARFI imaging methods were developed and used for the visualization of rapidly-moving myocardium with ARFI imaging. The following subsections describe these new methods and ARFI imaging sequences. A summary of all nonconventional ARFI imaging methods utilized in this paper, including two previously-implemented methods, is provided in table 1.

Parallel-transmit imaging

1. Parallel-transmit excitation—Cardiac ARFI imaging sequences in previous studies multiplexed the ARFI imaging sequences to shorten acquisition times.[17, 21] However, multiplexing higher-energy and longer excitation pulses resulted in a gradual weakening in the excitation pulses. As a result, a degree of interbeam radiation force variability between the multiplexed lines is present. To address this issue, a new technique of parallel-transmit excitation is employed, where ARFI excitation pulses are simultaneously transmitted along multiple lateral locations through the use of nonoverlapping apertures. In effect, the transducer aperture is divided into multiple separately-operated subapertures to simultaneously transmit three ARFI excitations.

2. Parallel-transmit tracking—As conventional B-mode transmit pulses typically use larger F/#s and smaller transmit apertures than ARFI excitations, the parallel-transmit imaging method was also implemented to transmit B-mode tracking lines in parallel and focus them about each parallel-transmit excitation. The parallel-receive locations were then centered about each M-mode line, and simultaneously recorded echoes along these lateral locations. As a result, displacement estimates were sampled at multiple lateral locations in parallel and without the need for multiplexing.

Pre-excitation displacement estimation

Previous studies into cardiac ARFI imaging have used interpolation-based quadratic motion filters to effectively reduce physiological motion artifacts to below 1 μm through the entire cardiac cycle.[23] These studies have also observed that at points of greater cardiac motion, such as during ejection or filling, physiological motion artifacts also increased. Quadratic motion filtering operates on a pixel-by-pixel basis and interpolates physiological motion with a least-squares, parabolic regression using an absolute reference point (t=0, d = 0) and displacement estimates made after an end-time threshold, selected by the user, where the tissue is assumed to have fully recovered from the ARFI excitation. This regression is then subtracted from the entire dataset to produce the ARFI-induced displacements.

New ARFI imaging sequences were developed that include multiple tracking lines directly preceding the reference line. As these tracking lines are recorded before transmission of the ARFI excitation, their displacements also provide an estimate of physiological motion in the absence of ARFI-induced motion and can therefore be used in the motion filter. A graphical representation of the quadratic motion filter including preexcitation displacement estimates is shown in figure 1.

New ARFI imaging sequences

Three-line M-mode ARFI, ECG-gated extended three-line M-mode ARFI and ECG-gated two-dimensional ARFI imaging sequences were developed for specific applications and to address various challenges of open-chest cardiac ARFI imaging. The following subsection describes these new sequences with a summary of these sequences and their sequence parameters presented in table 2.

1. Three-line M-mode ARFI imaging—Three-line M-mode ARFI imaging sequences are used to record myocardial stiffness through the entire cardiac cycle at high temporal sampling frequencies. As myocardial tissue has been observed to recover from an ARFI excitation within 2–3 ms, the maximum sampling rates for these sequences can exceed 300 Hz.[25] However, in order to limit tissue and transducer heating, M-mode ARFI lines are sampled at considerably-lower frequencies. The three-line M-mode images and plots presented in this paper were acquired at a sampling rate of 120 Hz.

Parallel-transmit excitation and tracking was implemented for these sequences to simultaneously transmit radiation force pulses and track displacements at multiple lateral locations. With a transmit F/# of 1.5 and focus of 1.5 cm, the M-mode lines were laterally spaced 1.31 cm apart to assure that the transmit apertures did not overlap.

Traditional M-mode imaging lines were also recorded at each lateral location at a sampling rate of 480 Hz during these acquisitions. From these data, all of the conventional measurements of M-mode image analysis were available. In this paper, incremental axial displacements were calculated using the same phase-shift estimation algorithm used to estimate axial displacements in ARFI imaging. Tissue-velocity estimates of the natural motion of the heart were then obtained by multiplying these incremental axial displacements by the traditional M-mode

imaging sampling frequency. B-mode images were also acquired within these sequences at a sampling rate of 30 Hz. Although not performed in this study, these B-mode images could be used to measure clinically-relevant metrics of cardiac imaging, such as chamber volumes, wall thicknesses and 2-D velocities, for comparative purposes.

2. ECG-gated extended three-line M-mode ARFI imaging—In order to observe transient changes of the heart across multiple heartbeats, ECG-gated extended three-line M-mode ARFI imaging sequences were developed. These sequences were derived from the three-line M-mode ARFI imaging sequences described in the previous section. Parallel-transmit excitation and tracking were implemented and the lateral spacing for the three M-mode lines was 1.31 cm. The sequences were focused at 1.5 cm with a transmit F/# of 1.5.

The ARFI imaging prf was reduced to extend the acquisition time. At these lower sampling rates, 2-D B-mode images were also acquired. To further prolong these acquisitions, the sequences were ECG-gated to record data for every other heartbeat. In total, 24 2-D B-mode and M-mode ARFI imaging frames were acquired on every other heartbeat across 17 beats. For a resting heart rate of 60 beats per minute (bpm), this would correspond to an imaging frame rate of 24 Hz.

3. ECG-gated two-dimensional ARFI imaging—ECG-gated two-dimensional ARFI imaging sequences were also developed. These sequences were based on the extended three-line M-mode ARFI imaging sequences as described in the previous section; however, through multiple consecutive heartbeats, the lateral locations of the three M-modes lines were electronically translated across a lateral field of view.

Using the parallel-transmit excitation method but not the parallel-transmit tracking method, these sequences simultaneously transmitted high intensity excitation pulses about three equally-spaced lateral locations and the four parallel-receive reference/tracking lines were multiplexed through the three parallel-ARFI excitation locations. As a result, displacement estimates were made along twelve lateral locations from each individual ARFI-excitation transmit. The ARFI imaging sequences repeatedly interrogated these twelve locations through a single heartbeat at ARFI imaging prfs that were determined by the heart rate. In total, twenty ARFI imaging frames were acquired within a single cardiac cycle.

The process was electronically translated to span a 24.7 mm lateral field of view, with a line density of 3.3 lines per millimeter, while ECG-gating the initiation of each successive ensemble of twelve tracking lines to a separate heartbeat. In total, the entire sequence of images was formed across nine heartbeats and interrogated 108 individual lateral locations. Multibeat synthesis was then used to reconstruct 2-D ARFI images of the heart through a single cardiac cycle. A diagram of this sequence is presented in figure 2.

III. EXPERIMENTAL PROCEDURE

Parallel-transmit imaging evaluation

A CIRS (Norfolk, VA) homogeneous tissue-mimicking phantom was imaged with three-line M-mode ARFI imaging sequences, which utilized either multiplexed imaging or parallel-transmit imaging. Single-line M-mode ARFI images centered about each lateral location were also acquired. The transmit foci and transmit F/#s were the same in all acquisitions. As the stiffness of the phantom was presumed to be constant and uniform, the displacement and recovery profiles of the phantom in response to a single excitation pulse were compared between the three sequences. Each M-mode sequence acquired data for 1 s at an ARFI imaging prf of 120 Hz. Repeated sampling within each acquisition was used for statistical analysis.

In vivo ARFI imaging of ovine subject

A thoracotomy was performed and the pericardium was cut away to expose the left side of an *ovine* heart. Pacing electrodes were sewn onto the left atrium, near the sinoatrial node, and onto the left ventricular free wall, near the apex. As a result, the heart could be paced at heart rates above the normal sinus rhythm from either the atria or ventricles.

In vivo cardiac images of the exposed heart were formed with the transducer placed into a vacuum apparatus and directly onto the epicardial surface of the heart. This apparatus employed suction to help the transducer maintain a single imaging plane within the heart and maintain a constant 1.0 cm axial distance away from the heart while holding an ultrasonically transparent standoff pad between the two. The transducer/vacuum apparatus was then centered atop the left ventricular free wall and oriented along the long axis of the heart. With this orientation, the left side of the image was closer to the base of the heart and the right side was closer to the apex and the ventricular pacing wire. While the heart was paced from either electrode, various images were then formed. In order to register the images with the cardiac cycle, the global ECG was recorded along with the voltage of the power supply on the scanner that was used to generate the ARFI excitations. The voltage of the pacing generator was also recorded.

1. Physiological motion filter performance analysis—While pacing from the leftventricle, a passive (zero-amplitude radiation force pulse) 2-D ARFI image of the heart was acquired at systole. The ARFI imaging sequence utilized parallel-receive and multiplexed imaging. However, as the sequences were passive acquisitions, there was no need to parallel-transmit ARFI excitations. Displacement data were filtered using the quadratic motion filter with and without including preexcitation displacement estimates. An end-time threshold of 3.75 ms was used in both cases. Using only the reference line and displacement estimates recorded only after the null excitation, two points of data beyond this end-time threshold were applied to the motion filter. A single displacement estimate, measured one tracking pulse repetition interval (PRI) before the reference line, was then added to the quadratic motion filter. The 2-D absolute valued ARFI images from both filters were then compared.

The performance of the quadratic motion filter through the cardiac cycle was then characterized using passive single-line M-mode ARFI imaging sequences. Again, displacement data were filtered using the quadratic motion filter with and without inclusion of pre-excitation displacement estimates. With a higher tracking prf than the 2-D sequences, six displacement estimates after the same end-time threshold were available for use in the quadratic motion filter. Three preexcitation displacement estimates were then added to the motion filter for comparison. From each filter, the average absolute ARFI-induced displacement curves through the entire thickness of the myocardium were calculated.

2. ARFI imaging sequence demonstration—While pacing from the left ventricle, the heart was imaged with active three-line M-mode ARFI imaging sequences. The ARFI imaging sequence utilized parallel-transmit excitation/tracking and was focused at an axial depth of 1.5 cm. The resulting ARFI-induced displacement curves were examined for uniformity in the displacement estimates through each lateral location and the entire cardiac cycle.

ECG-gated two-dimensional ARFI imaging sequences of the heart were then acquired. Although the sequences could have been gated to the QRS complex of the global ECG, as the heart was externally paced, the sequences were gated by the external pacing source. Again, the images were focused at a 1.5 cm axial depth. The spatial uniformity within each reconstructed 2-D ARFI image was examined. An average ARFI-induced displacement curve was also calculated to assess the spatial variability of this new sequence through the cardiac cycle.

The pacing source was then switched to the atrial electrode, and the heart was allowed to adjust to this new pacing location. Surgical tape was then wrapped around the superior and inferior venae cavae. ECG-gated extended three-line M-mode ARFI images of the heart were then acquired while occluding venous flow returning to the right atrium with surgical tape to induce decreasing preloads. These sequences were gated by the external pacing source, now stimulating from the atria. The displacement curves were inspected across multiple heartbeats for any changes that could be attributed to the decrease in preload.

IV. RESULTS

Parallel-transmit imaging evaluation

Three-line M-mode ARFI imaging acquisitions of a homogeneous phantom are shown in figure 3. As the sequences were designed for myocardial imaging, the total tracking time was insufficient to record the full displacement and recovery profile of the more compliant phantom. As a result, the displacement estimates were not motion filtered. Normalized displacements taken within a 1.9 mm axial kernel about the transmit focus and 0.66 ms after cessation of the radiation force pulse from each acquisition are shown in figure 3b. These displacements were normalized by the average measured displacement between the three M-mode lines. From this plot, the effects of multiplexing become apparent as a noticeable left-to-right drop in normalized displacements can be seen from the multiplexed acquisitions. Conversely, good agreement can be seen between the superimposed single-line M-mode and parallel-transmit acquisitions.

The averaged displacement profiles within a 1.9 mm kernel about the transmit focus for the multiplexed, parallel-transmit, and superimposed single-line M-mode acquisitions are shown in figures 3c–e, respectively. The regions of interest and lateral locations of these displacement profiles are shown in the B-mode image in figure 3a. The loss of temporal resolution due to multiplexed imaging is evident within the less sampled displacement plots in figure 3c. Additionally, the overall reduction in transmit power due to parallel-transmit excitation can be observed, as the ARFI-induced displacement profiles in figure 3d are smaller than the other two sequences.

In vivo ARFI imaging

1. Physiological motion filter performance analysis—The improvement due to the inclusion of preexcitation displacement estimates for the quadratic motion filter is demonstrated in the 2-D ARFI images taken during systole in figure 4. The matched B-mode image taken is shown in figure 4a. At this point of the cardiac cycle, the heart is contracting and there is considerable and complex physiological motion within the heart. The quadratic motion filtered images, taken 0.66 ms after cessation of the zero-amplitude excitation pulse, without and with preexcitation displacement estimates, are shown in figures 4b–c, respectively. Ideally, these images would be zero, indicating the complete removal of cardiac motion artifacts. The advantages in including preexcitation displacement estimates in the motion filter are evident within the images as the residual displacements are reduced and more uniform in figure 4c.

Average motion filtered absolute residual displacement plots from a passive, single-line M-mode ARFI imaging acquisition of an *ovine* left ventricular free wall *in vivo* is shown in figure 5. The lateral location and region of interest of the M-mode displacement plots are marked in the corresponding B-mode image, shown in figure 5a. Figure 5b displays residual displacement plots taken 0.71 ms after cessation of the null radiation force pulse and after application of the quadratic motion filter with and without including pre-excitation displacement estimates. The matched global ECG is shown in figure 5b, below the ARFI-induced displacement plot. The

ARFI-induced displacements indicate that the greatest residual displacements occurred at systole and about the QRS complex. However, by including pre-excitation displacement estimates in the quadratic motion filter, these systolic residual displacements are considerably reduced and physiological motion artifacts are seen to be below 0.2 μm throughout the entire cardiac cycle. The performances of the motion filters through diastole are comparable, with each filter reducing cardiac motion artifacts to below 0.15 μm.

2. ARFI imaging sequence demonstration—Three-line M-mode ARFI-induced displacement plots of an ovine left ventricular free wall are shown in figure 6. The corresponding B-mode image with the lateral positions and region of interest is shown in figure 6a. With the matched ECG shown below in figure 6d, figure 6b–c demonstrates the capabilities of the imaging sequence to produce three-line ARFI-induced displacement curves, averaged within a 1.9 mm axial kernel about the transmit focus and average tissue velocity curves, within a 1.9 mm axial kernel at the mid-myocardium. A benefit of parallel-transmit excitation can be seen in figure 6b, as the three ARFI-induced displacement estimates made at late diastole are similar, indicating nearly uniform diastolic elasticities within the regions of interest.

Within these M-mode plots, myocardial contraction is apparent with a sharp drop in ARFI-induced displacements and a rise in tissue velocity magnitudes at systole and shortly after application of the stimulating pulse (dashed vertical lines). Further, the apparent onset of myocardial contraction at all lateral locations seem to occur nearly coincidentally and at a specific time of the cardiac cycle. By contrast, the waveforms of each M-mode plot are less similar through diastole, particularly at the rightmost (triangle plot) M-mode line, suggesting that diastolic relaxation may occur in a less spatially-coordinated manner than myocardial contraction.

A single matched B-mode and ARFI image frame, reconstructed from an ECG-gated 2-D ARFI imaging sequence, is shown in figure 7. The spatial continuity within the B-mode image in figure 7a suggests that the behavior of the heart was widely stable and repeatable across the nine heartbeats of the acquisition. The ARFI image in figure 7b, taken right at the onset of ventricular systole, shows a region of myocardium with relatively-uniform ARFI-induced displacements laterally and little indication of a multiplexing artifact that would be manifested as discontinuities within each third of the image. By transmitting the ARFI excitation with a relatively small F/# of 1.5, a focal gain in ARFI-induced displacements can be observed through the depth of the myocardium as displacements are large within the epicardium and near the focus but fall rapidly through the depth of the myocardium and towards the endocardial surface.

The exact point of acquisition within the cardiac cycle of the selected B-mode and ARFI images is marked in figure 7c by the starred points in the ARFI-induced displacement curve and its matched global ECG. This ARFI-induced displacement curve was calculated by averaging displacements measured across the entire 3.1 cm lateral field of view and a 0.19 cm axial field of view centered about the 1.5 cm transmit focus. The error bars within this displacement plot correspond to the lateral spatial variability within this region of interest, as marked by the two horizontal lines in the B-mode image in figure 7a. The plot also demonstrates the same cyclic behavior observed within the previous three-line M-mode ARFI image. Additionally, as the difference between the minimum systolic and maximum diastolic ARFI-induced displacements exceeds the margin of their errorbars, this cyclic variation is likely not an artifact caused by spatial variability.

ECG-gated extended three-line M-mode ARFI images of a left-ventricular free wall while occluding the superior and inferior venae cavae are shown in figure 8. The matched B-mode image, with the lateral positions and regions of interest of the three M-mode lines, is shown in figure 8a. ARFI-induced displacements were averaged within a 3.8 mm axial kernel, starting

from the epicardial surface. In figure 8b, with the matched ECG below, a beat-to-beat analysis of the center M-mode line indicates that the end-diastolic ARFI-induced displacements increased during the occlusions and, therefore, the myocardium was more compliant at diastole due to the decrease in preload. The end-systolic displacements remained relatively constant and therefore suggested the end-systolic stiffness was unaffected by changes in preload. As the heart was atrially paced during this acquisition, a pacing artifact (rather than a normal P-wave) is present within the ECG at the beginning of each beat and atrial systole. Individual inspections of the first and last heartbeats for the left, center, and right lateral locations, shown in figures 8c–e, respectively, corroborate these results.

V. DISCUSSION

Among the three methods of three-line M-mode imaging presented in this paper, superimposing the three single-line M-mode acquisitions of a homogeneous phantom produced the best-sampled images with the largest ARFI-induced displacements. A clinical realization of this sequence requires ECG-gating and multibeat synthesis in order to temporally register the M-mode lines. As demonstrated in figure 3, although parallel-transmit excitation reduced the effective pushing strength at each individual excitation, the uniformity of the push and ability to track displacements in parallel allow *in vivo* interbeam comparisons of local myocardial elasticities. Also, by tracking in parallel without multiplexing, there was greater flexibility in frame selection and for parametric analyses of the data. Finer temporal sampling also provided additional displacement estimates for the physiological motion filters and, therefore, could help further reduce motion artifacts within the images.

Perhaps the most advantageous effect of parallel-transmit excitation was that displacements could be tracked more immediately after cessation of the radiation force pulse. As a result, the sequences were capable of observing the initial response of the tissue to the radiation force pulse. This benefit can be seen within the displacement and recovery profiles in figure 3b, as the multiplexed sequences were only able to track the homogeneous phantom in recovery and therefore the true maximum displacement was not observed.

The parallel-transmit sequences did not exactly reproduce the displacement and recovery profiles at each of the three M-mode lines. However, as similar displacement and recovery profile variations were also observed within the superimposed single-line M-mode acquisitions, it is likely that these differences were caused by factors external to the ARFI imaging sequences, possibly pertaining to variability related to the transducer and the local elasticities within the phantom.

In order to perform parallel-transmit imaging, the lateral spacings between the multiple transmit locations must be sufficiently large to accommodate the desired F/#s and transmit foci. However, these spacings are also limited by the size of the transducer aperture. As a result, parallel-transmit imaging is most applicable when using large, linear-array transducers while imaging superficial organs and structures including the thyroid, breast and superficial blood vessels. For transthoracic cardiac ARFI imaging, where phased array probes are more commonly used, parallel-transmit excitation may not be a viable method.

Noninvasive transthoracic cardiac ARFI imaging has previously been demonstrated to be capable of observing cyclical variations in ARFI-induced displacements that reflected the expected changes in myocardial stiffness through the cardiac cycle.[26] However, preliminary initial results also indicated that the ARFI images contained greater physiological motion artifacts. Additionally, the ability to generate measurable displacements within all regions of the cardiac cycle is another challenge, as the limited number of transthoracic viewing angles of the heart places certain regions of myocardium at considerable depths.

The three-line M-mode image in figure 5b demonstrates that average absolute residual displacement artifacts were below 0.35 μm through the entire cardiac cycle. With diastolic ARFI-induced tissue displacements above 10 μm in all active ARFI imaging acquisitions, these levels of motion artifact are sufficiently low to make accurate stiffness comparisons within the ARFI image. In the 2-D ARFI image in figure 4, the levels of motion artifact are satisfactorily low in the proximal regions of the myocardium that are more relevant to epicardial ARFI imaging. However, significant levels of residual displacement are present in the distal portions of the 2-D ARFI image. This increase in error at depth can likely be attributed to the vacuum apparatus. As the apparatus held the transducer over a fixed region of myocardium, the transducer was able to move in unison with the epicardium. As a result, regions of myocardium proximal to the vacuum apparatus and transducer would appear more stationary within the images and, therefore, contain smaller amounts of physiological motion and motion artifacts.

The performance improvement of the motion filter with the inclusion of preexcitation displacement estimates can likely be attributed to the increased accuracy of the displacement estimates at these earlier time steps. With displacement estimates made after an end-time threshold, there is greater time for the tissue to move off axis, and these data are more likely to decorrelate from the initial reference line. The Cramer-Rao lower bound indicates that the minimum displacement estimate error (jitter) associated with time-delay estimators is inversely related to the correlation coefficient.[27] Therefore, displacements at these later time steps are likely to have increased jitter and error within the ARFI images. As interpolation-based motion filters rely on these data to approximate physiological motion, any error within the displacement estimates will transfer to the motion filter and therefore the ARFI images. Conversely, displacement estimates at earlier time steps are more likely to have higher correlation coefficients and smaller jitter as the tissue has less time to move out of the tracking beam. As a result, the interpolation-based motion filters are able to more effectively remove physiological cardiac motion artifacts from the ARFI images.

Several studies have investigated cardiac strain imaging to measure electromechanical propagation within the heart.[28,29] The potential of ARFI imaging to track a corollary mechanical wave of stiffness is demonstrated in figures 6 and 7. The ARFI imaging sequences associated with these figures are capable of observing variations within the local tissue elasticities with sufficient temporal resolution to estimate timing delays between the ARFI-induced displacement curves at each lateral location. This is apparent within the ARFI-induced displacement plots, as myocardial stiffening within the right M-mode line (triangle plots) appears to lead the other two. With the right side of the image proximal to the pacing wires, this result may reflect the propagation of mechanical stiffness across the field of view and away from the pacing source.

Stiffness propagation may also be extrapolated from the two-dimensional ARFI imaging sequences, where the additional spatial information may provide complementary data to the three-line M-mode images. Although variations within the two-dimensional images can be attributed to many sources, one possible contributor to the error bars in figure 7c is timing differences within the field of view associated with a propagating stiffness wave. Further investigations with the ARFI imaging sequences described in this paper are warranted to investigate the feasibility of ARFI imaging in measuring stiffness and electromechanical propagation through the heart.

Previous 2-D ARFI imaging sequences involved the acquisition of multiple 2-D ARFI images at low sampling rates (10 Hz) across 4–5 heartbeats. These images were then rearranged based on their relative times of acquisition within the cardiac cycle to form a sequence of ARFI images of a single heartbeat.[17] A consequence of this method is that the effective prfs between each frame were variable. Additionally, this sequence of ARFI images provided no temporal

continuity. As a result, estimation of the amount and rates of myocardial stiffening and relaxation were problematic. In contrast, as the new sequences gated the acquisitions into three-line M-mode sub-images, the ARFI-induced displacement estimates at each individual lateral location were regularly sampled at constant prfs and came from a single heartbeat.

ECG-gated extended three-line M-mode ARFI imaging sequences were designed to investigate the feasibility of ARFI imaging-based measurement of myocardial function and performance. The ARFI-induced displacement plots demonstrate the capabilities of this new sequence to track gradual, beat-to-beat changes in myocardial elasticity through multiple heartbeats. As a result, the transient changes in myocardial stiffness under various loads and operating conditions can be recorded. The three M-mode lines also provide spatial sensitivity not available with pressure-volume analysis, the current clinically-accepted method for measuring left ventricular function.

The M-mode ARFI images presented within this paper were formed after being axial averaged and temporally mean filtered. As a result, the presented ARFI-induced displacement plots contained reduced displacement artifacts and noise while sacrificing high-frequency resolution. This trade-off was considered acceptable, as the intended purpose of this paper was simply to demonstrate these new ARFI imaging methods and sequences. However, these image processing methods may remove clinically-relevant data, particularly during ventricular contraction, when myocardial stiffening appears to occur rapidly and within a short period of time. Less aggressive low-pass filtering may preserve this information; however, the accompanying decrease in SNR must be addressed.

Similarly, spatial averaging and median filtering suppressed high-frequency content within the 2-D ARFI images. However, as these were healthy hearts, there was no reason to suspect large and sudden heterogeneities in stiffness within the field of view, and the high-frequency content removed from these images was likely to be predominantly noise. Nevertheless, in various applications where sharp and distinct variations of stiffness may be present, such as for the visualization of infarctions or myocardial ablations, these signal processing techniques will be optimized to properly assess the extent of these regions.

The sequences developed provide ARFI-induced displacement curves, which reflect myocardial stiffnesses. However, the fundamental challenge of quantitatively relating ARFI-induced displacements to myocardial stiffness remains. Propagation velocities, stiffness ratios and normalized rates of stiffening can be extracted from these data without knowing the exact displacement-to-stiffness conversion. However, as both diastolic and systolic stiffnesses can be variable, the clinical utility of these metrics remains uncertain. Investigations into shear wave elasticity (SWEI) and shear wave velocimetry have produced quantitative measures of elasticity that could also be applied to cardiac imaging.[30–34] However, these imaging modalities rely on the propagation of slowly propagating (1–4 m/s), mechanical waves and may not be suited for dynamic environments such as the heart.

VI. CONCLUSION

Novel ARFI imaging sequences were developed for superficial organ imaging investigations. These sequences utilized parallel-transmit excitation, parallel-transmit tracking, pre-excitation tracking, parallel-receive, ECG-gating, multibeat synthesis and multiplexing to form quality ARFI images at all points of cardiac cycle. The resultant ARFI-induced displacement curves provided new information into myocardial elasticity with high temporal and spatial resolution previously not available. Additionally, the accuracy of ARFI-induced displacement estimation was improved. With these new sequences and the improved ARFI images, various quantitative applications of cardiac ARFI imaging can be investigated.

Acknowledgments

This research was funded by NIH Grant #s: R01-HL-075485, R01-CA-114093 and R21-EB-007741. We would like to thank Siemens Medical Solutions USA, Inc. for their hardware and system support. We would also like to thank Joe Owen, Mark Palmeri, Stephanie Eyerly, Ashley Li, Stephen Rosenzweig, Muyinatu Lediju, Aine Tierney, Ned Danieley, David Bradway, Jeremy Dahl, Liang Zhai, Elien Dixon-Tulloch, Martha Absher and Kathryn Nightingale.

References

1. Nyborg, W. Acoustic streaming. In: Mason, W., editor. Physical Acoustics. Academic Press, Inc; New York: 1965. p. 265-331.
2. Palmeri M, Sharma A, Bouchard R, Nightingale R, Nightingale K. A finite-element method model of soft tissue response to impulsive acoustic radiation force. IEEE Trans Ultrason Ferroelectr Freq Control 2005;52:1699–1712. [PubMed: 16382621]
3. Torr G. The acoustic radiation force. Amer J Phys 1984;52:402–408.
4. Nightingale K, Bentley R, Trahey G. Observations of tissue response to acoustic radiation force: opportunities for imaging. Ultrasonic Imaging 2002;24:100–108. [PubMed: 12199416]
5. Nightingale K, Soo M, Nightingale R, Trahey G. Acoustic radiation force impulse imaging: *In vivo* demonstration of clinical feasibility. Ultrasound Med Biol 2002;28:227–235. [PubMed: 11937286]
6. Vedam S, Kini V, Keall P, et al. Quantifying the predictability of diaphragm motion during respiration with a noninvasive external marker. Med Phys 2003;30:505–513. [PubMed: 12722802]
7. Fahey B, Palmeri M, Trahey G. The impact of physiological motion on tissue tracking during radiation force imaging. Ultrasound Med Biol 2007;33:1149–1166. [PubMed: 17451869]
8. Fahey B, Nightingale K, Nelson R, Palmeri M, Trahey G. Acoustic radiation force impulse imaging of the abdomen: demonstration of feasibility and utility. Ultrasound Med Biol 2005;31:1185–1198. [PubMed: 16176786]
9. Gorcsan J, Strum D, Mandarino W, Pinsky M. Color-coded tissue Doppler assessment of the effects of acute ischemia on regional left ventricular function: comparison with sonomicrometry. J Am Soc Echocardiogr 2001;14:335–342. [PubMed: 11337678]
10. McVeigh E. MRI of myocardial function: motion tracking techniques. Magn Reson Imaging 1996;14:137–150. [PubMed: 8847969]
11. Ritchie C, Godwin J, Crawford C, et al. Minimum scan speeds for suppression of motion artifacts in CT. Radiology 1992;185:37–42. [PubMed: 1523332]
12. Benetos A, Laurent S, Hoeks A, Boutouyrie P, Safar M. Arterial alterations with aging and high blood pressure. A noninvasive study of carotid and femoral arteries. Arterioscler Thromb 1993;13:90–97. [PubMed: 8422344]
13. D'hooge J, Konofagou E, Jamal F, et al. Two-dimensional ultrasonic strain rate measurement of the human heart in vivo. IEEE Trans Ultrason Ferroelectr Freq Control 2002;49:281–286. [PubMed: 11885685]
14. Konofagou E, D'hooge J, Ophir J. Myocardial elastography–a feasibility study in vivo. Ultrasound Med Biol 2002;28:475–482. [PubMed: 12049961]
15. Dumont D, Dahl J, Miller E, et al. Lower-limb vascular imaging with acoustic radiation force elastography: Demonstration of *In vivo* feasibility. IEEE Trans Ultrason Ferroelectr Freq Control 2009;56:931–944. [PubMed: 19473912]
16. Fahey B, Hsu S, Wolf P, Nelson R, Trahey G. Liver ablation guidance with acoustic radiation force impulse imaging: Challenges and opportunities. Phys Med Biol 2006;51:3785–3808. [PubMed: 16861781]
17. Hsu S, Fahey B, Dumont D, Wolf P, Trahey G. Challenges and implementation of radiation force imaging with an intra-cardiac ultrasound transducer. IEEE Trans Ultrason Ferroelectr Freq Contr 2007;54:996–1009.
18. Trahey G, Palmeri M, Bentley R, Nightingale K. Acoustic radiation force impulse imaging of the mechanical properties of arteries: in vivo and ex vivo results. Ultrasound Med Biol 2004;30:1163–1171. [PubMed: 15550320]

19. Fahey B, Palmeri M, Trahey G. Frame rate considerations for abdominal acoustic radiation force impulse imaging. Ultrasonic Imaging 2006;28:193–210. [PubMed: 17521042]
20. Palmeri M, Frinkley K, Nightingale K. Experimental studies of the thermal effects associated with radiation force imaging of soft tissue. Ultrasonic Imaging 2004;26:29–40. [PubMed: 15134392]
21. Bouchard R, Dahl J, Hsu S, Trahey G. Image quality, tissue heating, and frame-rate trade-offs in acoustic radiation force impulse imaging. IEEE Trans Ultrason Ferroelect Freq Contr 2009;56:63–76.
22. Dahl J, Pinton G, Palmeri M, et al. A parallel tracking method for acoustic radiation force impulse imaging. IEEE Trans Ultrason Ferroelectr Freq Contr 2007;54:301–312.
23. Hsu S, Bouchard R, Dumont D, Wolf P, Trahey G. In vivo assessment of myocardial stiffness with acoustic radiation force impulse imaging. Ultrasound Med Biol 2007;33:1706–1719. [PubMed: 17698282]
24. Kasai C, Namekawa K. Real-time two-dimensional blood flow imaging using an autocorrelation technique. IEEE Trans Ultrason Ferroelectr Freq Contr 1985;32:458–163.
25. Fahey B, Nightingale K, Wolf P, Trahey G. Acoustic radiation force impulse imaging of myocardial radio-frequency ablation: Initial in vivo results. IEEE Trans Ultrason Ferroelectr Freq Contr 2005;52:631–641.
26. Bradway D, Hsu S, Fahey B, Dahl J, Nichols T, Trahey G. Transthoracic cardiac ARFI: a feasibility study. Proc IEEE Ultrason Symp 2007:448–451.
27. Walker W, Trahey G. A fundamental limit on delay estimation using partially correlated speckle signals. IEEE Trans Ultrason Ferroelectr Freq Contr 1995;42:301–308.
28. Faris O, Evans F, Ennis D, et al. Novel technique for cardiac electromechanical mapping with magnetic resonance imaging tagging and an epicardial electrode sock. Ann Biomed Eng 2003;31:430–440. [PubMed: 12723684]
29. Pernot M, Fujikura K, Fung-Kee-Fung S, Konofagou E. ECG-gated, mechanical and electromechanical wave imaging of cardiovascular tissues in vivo. Ultrasound Med Biol 2007;33:1075–1085. [PubMed: 17507146]
30. Bercoff J, Tanter M, Fink M. Supersonic shear imaging: a new technique for soft tissue elasticity mapping. IEEE Trans Ultrason Ferroelectr Freq Contr 2004;51:396–409.
31. Kruse S, Smith J, Lawrence A, et al. Tissue characterization using magnetic resonance elastography: preliminary results. Phys Med Biol 2000;45:1579–1590. [PubMed: 10870712]
32. Manduca A, Oliphant T, Dresner M, Mahowald J, Kruse S, Amromin E, Felmlee J, Greenleaf J, Ehman R. Magnetic resonance elastography: Non-invasive mapping of tissue elasticity. Med Image Anal 2001;5:237–254. [PubMed: 11731304]
33. Palmeri M, Wang M, Dahl J, Frinkley K, Nightingale K. Quantifying hepatic shear modulus in vivo using acoustic radiation force. Ultrasound Med Biol 2008;34:546–558. [PubMed: 18222031]
34. Sarvazyan A, Rudenko O, Swanson S, Fowlkes J, Emelianov S. Shear wave elasticity imaging: a new ultrasonic technology of medical diagnostics. Ultrasound Med Biol 1998;24:1419–1435. [PubMed: 10385964]

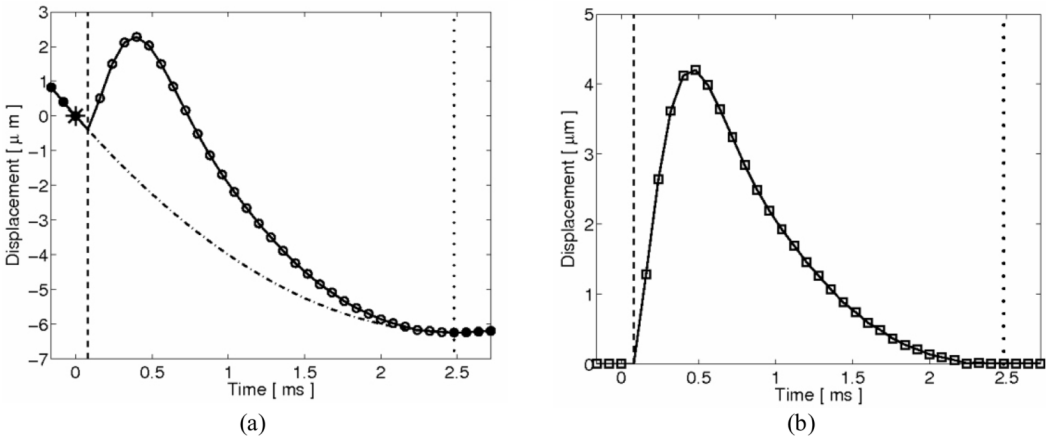

FIG. 1.

Graphical representation of the interpolation-based quadratic motion filter with the inclusion of preexcitation displacement estimates. (a) ARFI imaging displacement estimates (circle plot), measured via delay estimation between a single reference M-mode line and multiple successive M-mode lines, include ARFI-induced tissue displacements along with physiological cardiac motion. A quadratic function (dashdotted line) passing through the origin (starred point) is fit to a subset of displacement estimates (solid circle points) taken before transmission of the radiation force pulse (dashed line) and after an end-time threshold (dotted line). This quadratic function is then subtracted from the data at all times to obtain (b) the motion-filtered ARFI-induced displacement and recovery profile (square plot).

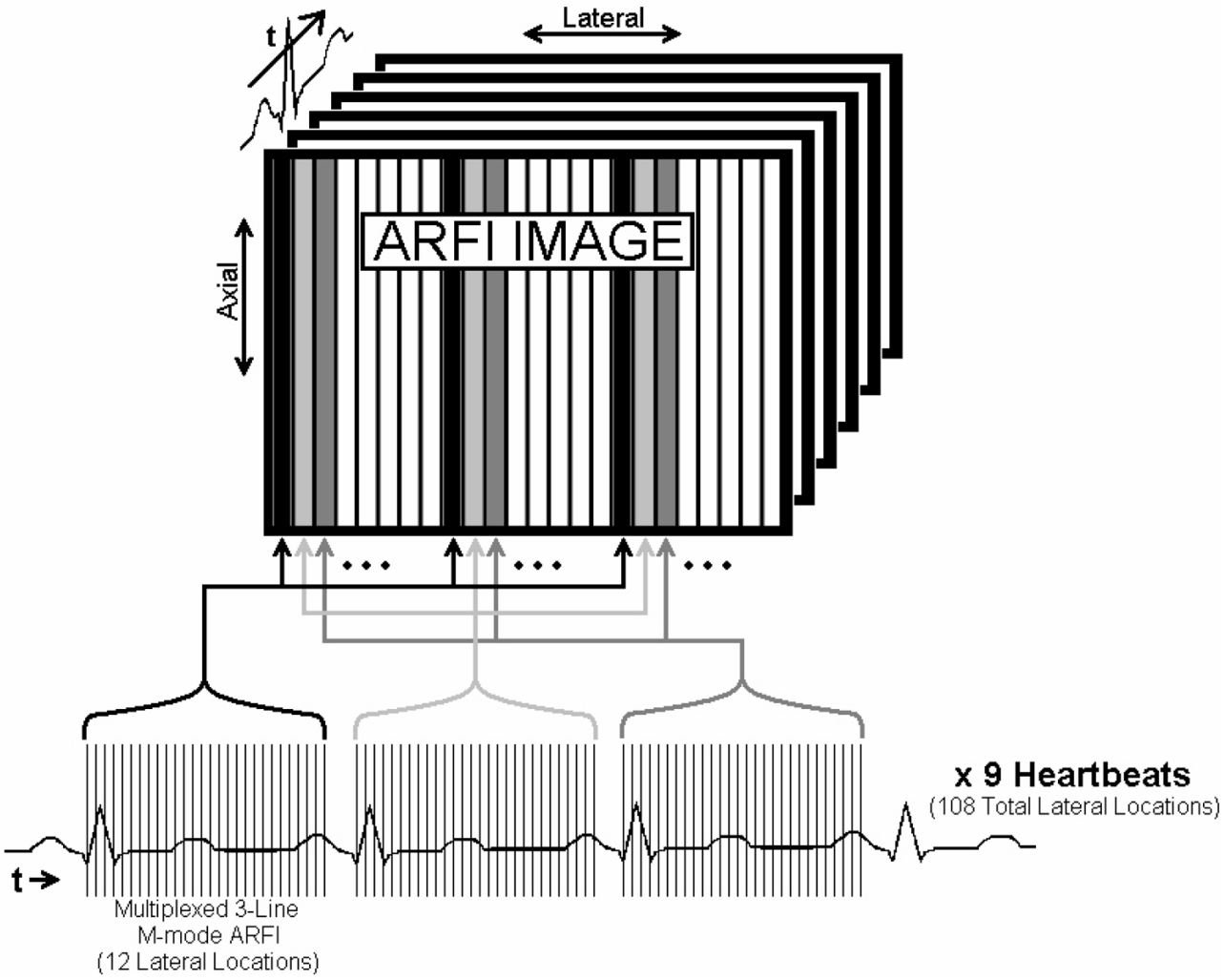

FIG. 2.

Graphical depiction of an ECG-gated two-dimensional ARFI imaging sequence. Across nine consecutive heartbeats, M-mode ARFI images were repeatedly sampled at twelve lateral locations, multiplexed in quatrains about three excitations regions and separated one-third of the field of view apart. On successive heartbeats, the excitation and tracking locations were then electronically translated across the field of view. At the end of the acquisition, multibeat synthesis was used to reconstruct a sequence of two-dimensional ARFI images through a single cardiac cycle.

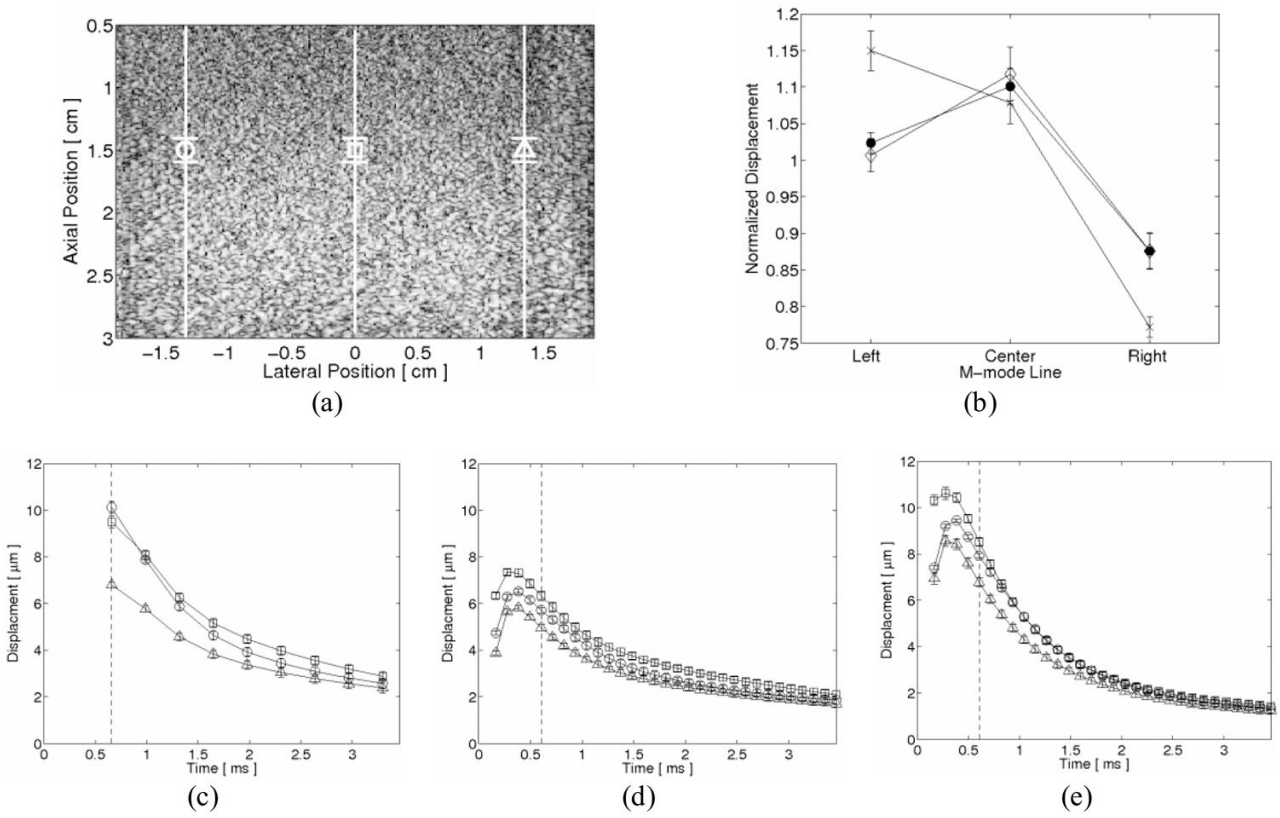

FIG. 3.

Three-line M-mode ARFI imaging of a homogeneous phantom. (a) The B-mode image marks the lateral locations and regions of interest for each M-mode line by their respective shapes. (b) Normalized displacements measured at the first commonly-recorded tracking time (dashed line in c–e) show good agreement between the superimposed single M-mode line acquisitions (solid circle plot) and the three-line parallel-transmit excitation/tracking M-mode acquisition (diamond plot). Due to power supply limitations, the corollary three-line multiplexed M-mode imaging acquisition (*x* plot) exhibits a progressive left-to-right drop in normalized displacements. The tradeoffs associated with parallel-transmit excitation/tracking are evident when comparing the individual M-mode line displacement profiles from (c) the multiplexed, (d) parallel-transmit and (e) superimposed single-line ARFI imaging acquisitions. Although an overall decrease in displacement magnitudes is observed, parallel-transmit imaging allows for finer and more immediate temporal sampling after cessation of the radiation force pulse.

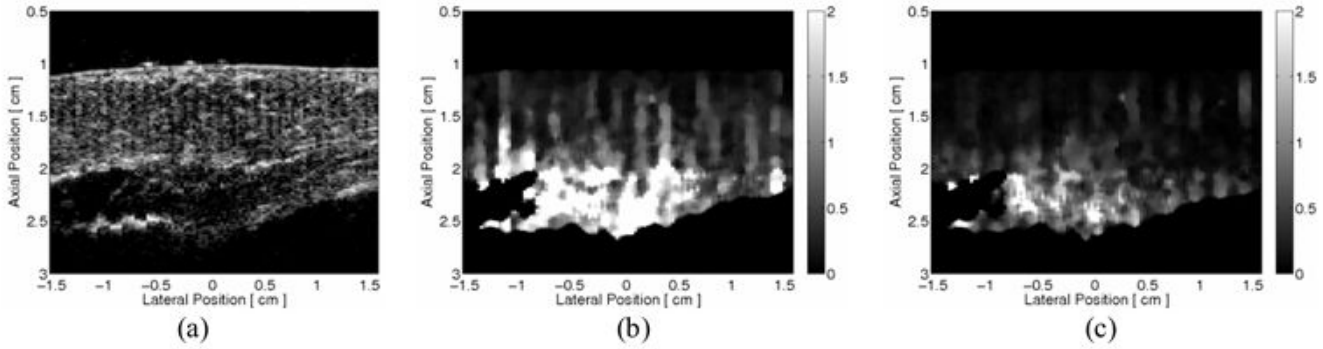

FIG. 4.

In vivo two-dimensional ARFI imaging demonstration of the improvement of the quadratic motion filter by including pre-excitation displacement estimates. From a passive ARFI imaging acquisition, absolute residual displacement images (ìm away from the transducer), taken 0.66 ms after cessation of the zero-amplitude radiation force pulse, were formed at systole. (a) The B-mode image shows a section of left ventricular myocardium located near the apex. By motion filtering with displacement estimates taken only after the end-time threshold, (b) the residual displacement ARFI image contains considerable physiological motion artifacts, as an appreciable amount of the image is non-zero. By including pre-excitation displacement estimates in the quadratic motion filter, physiological motion artifacts are markedly reduced, as (c) the corresponding residual displacement ARFI image has become more uniform and closer to zero.

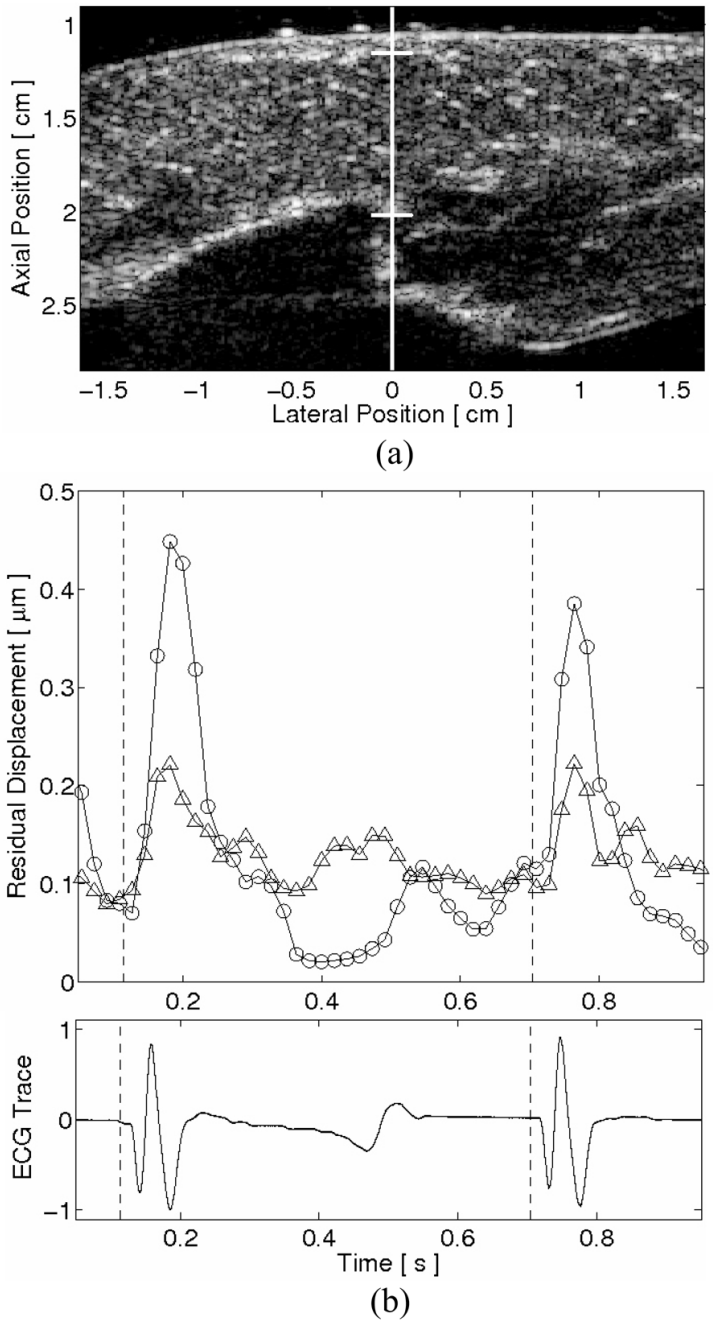

FIG. 5.

Average absolute residual displacements within an *in vivo* single line M-mode ARFI image of the left ventricular free wall. The lateral position and region of interest of the M-mode ARFI line are marked within (a) the matched B-mode image. After motion filtering, (b) the average absolute residual displacement plots indicate that the inclusion of preexcitation displacements (triangle points) better estimates physiological motion at systole than motion filtering with only postexcitation displacement estimates (circle points). The performances of the motion filters at diastole are comparable. The matched global electrocardiogram is shown below.

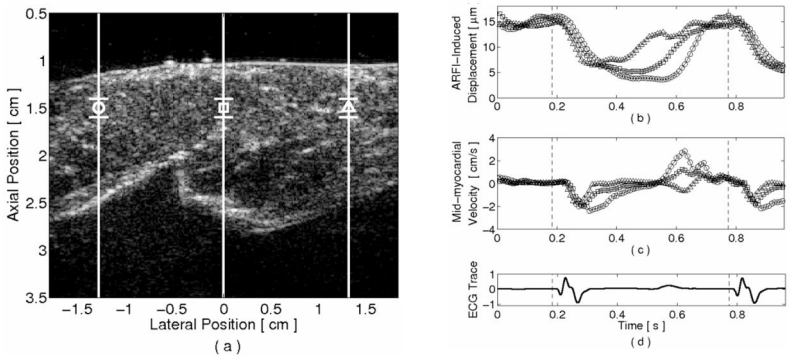

FIG. 6.

Three-line M-mode ARFI-induced displacement plots of an externally-paced *ovine* left-ventricular free wall. The lateral positions and regions of interest are marked by their respective shapes within (a) the corresponding B-mode image. With this acquisition, (b) parallel ARFI-induced displacement curves and (c) mid-myocardial tissue velocities can be calculated simultaneously at three lateral locations. (d) The matched global ECG is shown below and the application of the pacing stimulus is marked by the dashed vertical lines. Diastolic ARFI-induced displacements at all three curves are comparable due to the implementation of parallel-transmit excitation. The displacement and tissue velocity plots indicate that there is sufficient temporal resolution within these sequences to extract systolic phase delays between the three lateral locations

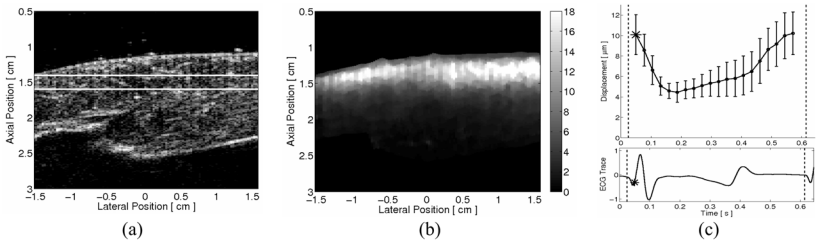

FIG. 7.

A single (a) B-mode and (b) ARFI image frame from an ECG-gated two-dimensional ARFI imaging acquisition of an externally-paced *ovine* left ventricle. The point of the cardiac cycle at which this specific frame was acquired is marked by the starred point in (c) the ARFI-induced displacement curve and the matched global ECG below. The ARFI-induced displacement curve was calculated by spatially averaging displacements (μm away from the transducer) measured within the region of interest, as marked on the B-mode image by the two horizontal lines. Error bars within the plot indicate that images are relatively homogeneous, with spatial variations in ARFI-induced displacement ranging from 2–4 μm.

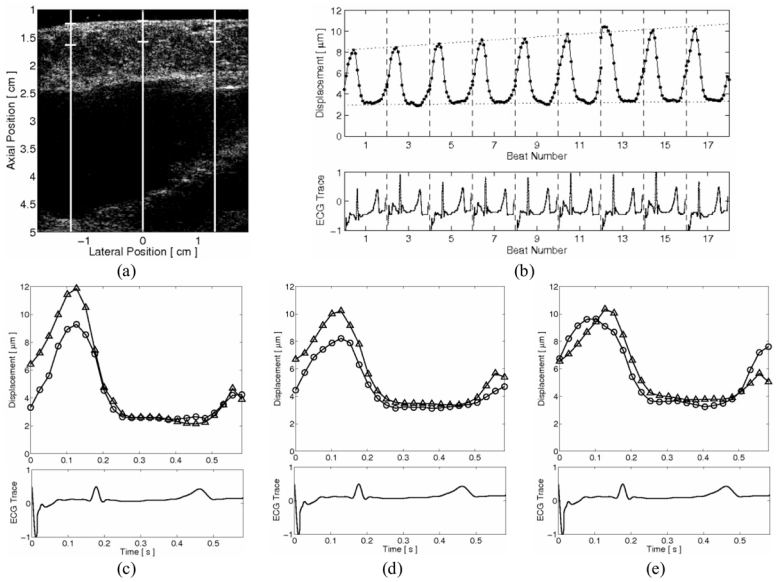

FIG. 8.

ECG-gated extended three-line M-mode ARFI image of a left ventricular free wall during venal caval occlusions. The lateral locations and regions of interest are marked within (a) the corresponding B-mode image. With the matched global ECG below, (b) the ARFI-induced displacement curve of the center lateral location shows diastolic displacements increased, indicating a decrease in diastolic stiffness as the preload decreases. The end-systolic displacements remained unchanged, suggesting that the end-systolic stiffness was preload independent. This trend can also be observed within the individual ARFI-induced displacement plots between the first (circle plots) and last (triangle plots) heartbeats for the (c) left, (d) center and (e) right lateral locations.

TABLE 1

Summary of nonconventional ARFI imaging methods used in this paper.

Method	Description	Intended benefit
Previously implemented		
Parallel-receive[22]	Simultaneously records echoes from multiple lateral locations.	Shortens acquisition time; reduces number of excitations.
Multiplexed imaging[21]	Multiplexes transmit/receive position through multiple nonadjacent lateral locations.	Shortens acquisition time while sacrificing tracking prf.
Newly implemented		
Parallel-transmit excitation	Simultaneously transmits ARFI excitations at multiple nonadjacent lateral locations.	Alternative to multiplexing; allows for more uniform excitation across each lateral location.
Parallel-transmit tracking	Simultaneously transmits B-mode transmit pulses at multiple nonadjacent lateral locations	Alternative to multiplexing; does not significantly shorten acquisition time but preserves tracking prf.
Pre-excititation displacement estimation	Records multiple displacement estimates before the transmission of the radiation force pulse.	Improve motion filter performance.

TABLE 2

New ARFI imaging sequence summary.

	Three-line M-mode	ECG-gated extended three-line M-mode	ECG-gated two-dimensional
Sequence parameter			
Acquisition time (heartbeats)	1–3	17	9
Number of lateral locations	3	3	108
Lateral beam spacing (mm)	13.1	13.1	0.30
ARFI imaging prf	120 Hz	24 samples/beat	20 samples/beat
Sequence description	Three-line M-mode ARFI with high temporal resolution.	Three-line M-mode ARFI across multiple heartbeats for beat-to-beat analysis.	Synthetically-created 2-D ARFI images with high spatial resolution.